WILEY | Hindawi

Research Article

Hierarchical Coordinated Control of DC Microgrid Based on Recursive Fuzzy Neural Network Algorithm

Haotian Wu [1,2] **Zhong Wei,**[1] **Shiwen Liu,**[3] **and Ming Shi**[1]

[1]*Shanghai Investigation, Design & Research Institute Co., Ltd, Shanghai 200335, China*
[2]*North China Electric Power University, Beijing 102206, China*
[3]*Shanghai University of Electric Power, Shanghai 200000, China*

Correspondence should be addressed to Haotian Wu; 50201603@ncepu.edu.cn

In order to realize the stable operation of the DC microgrid, a hierarchical coordinated control method of the DC microgrid based on the recursive fuzzy neural network algorithm is designed in this article. Based on the analysis of the working mode and topology of the DC microgrid, the droop control coefficient is calculated through power flow calculation, and then, a three-layer control strategy is designed combined with a hierarchical coordinated control algorithm to realize the distributed coordinated control of DC microgrid. Combined with the recursive fuzzy neural network algorithm, the real-time amplitude limiting and convergence of the output of the distributed coordination controller are realized. Experimental results show that under the control of this method, the changes in current and voltage at each port of the DC microgrid are relatively stable during off-grid switching. In addition, this method effectively reduces the fault rate of power grid lines, which fully proves the feasibility and reliability of this method.

1. Introduction

With the increasing proportion of renewable energy such as solar energy and wind energy connected to the power grid, microgrid has been widely used as an important form of distributed energy access [1]. Since the microgrid contains a large number of DC power supplies, such as photovoltaic, fuel cells, and energy storage, as well as DC loads, such as LED lighting and electric vehicles, the traditional AC microgrid needs the connection of commutators to access these power supplies and loads, which increases the cost and loss. Therefore, in recent years, the DC microgrid has attracted more and more attention from academic and industrial circles at home and abroad [2]. With the continuous development of power electronics technology, insulated gate bipolar transistor (IGBT) and digital signal processing (DSP) appear one after another. A voltage source converter (VSC) is mainly composed of IGBT, and its control system is mainly composed of DSP. VSC can be self-commutating without an AC system providing commutation voltage. Secondly, VSC can independently control the output of active

and reactive power through IGBT. Finally, when the power flow reverses, the direction of DC current reverses, and the DC voltage remains unchanged. This is the theoretical basis of parallel multiterminal flexible DC (VSC-MTDC). Nowadays, VSC-MTDC is the main topology of the DC microgrid. The construction of a DC microgrid based on VSC-MTDC is an effective way to solve DC load grid connection and DC power consumption [3].

The multiterminal DC microgrid based on VSC-MTDC has high control ability and flexibility compared with the traditional AC microgrid, but its operation control strategy is relatively complex. In particular, the control of DC voltage is the most important control goal of a multiterminal DC microgrid because it is related to the stability of DC power flow. At present, the mainstream control strategies of multiterminal DC microgrids are mainly divided into two categories: one is single-point DC voltage control, and the other is multipoint DC voltage control. Among them, single-point DC voltage control is divided into master-slave control and voltage margin control, and multipoint DC voltage control is divided into voltage slope control and segmented voltage

slope control [4]. Based on the background of multiterminal flexible DC transmission, Reference [5] discusses the development status and main control modes of multiterminal DC microgrid and discusses the advantages and disadvantages, existing problems, and protection methods of various control modes. Reference [6] designed the DC microgrid distributed coordination method based on finite time consistency. In this control method, voltage secondary control and power generation cost operation control are introduced based on the original droop control, and each power generation unit is only communicated with the adjacent communication unit, and multiple control objectives such as voltage stability and power generation cost minimization are achieved by the finite time consistency algorithm. In Reference [7], a multisource coordinated control method for DC microgrid based on virtual voltage is designed. Combined with the idea of virtual voltage and autonomous decentralized control, this method firstly analyzes the influence of line resistance on current-sharing control in detail, proposes a current-sharing control strategy based on virtual voltage, and then proposes an improved dynamic consistency algorithm, which can dynamically track and control the busbar voltage at the outlet of each converter and quickly converge the consistent value.

In the past few years, the neural network has been used to identify and control the real-time value of a nonlinear system, and the DC microgrid is essentially a nonlinear input-output system. The recursive fuzzy neural network (RFNN) combines many advantages of recurrent neural network (RNN) and fuzzy control. It has the advantages of low-level learning and computing ability, as well as high-level human-like thinking and reasoning of fuzzy theory. Reference [8] proposed a servo-driven adaptive hybrid control system of permanent magnet synchronous motor (PMSM) based on self-evolving fuzzy neural network (RRSEFNN) based on recursive radial basis function network (RBFN). RRSEFNN combines the advantages of the self-evolving fuzzy neural network, recursive neural network, and RBFN. The simulation results show that this method has accurate dynamic response ability. In Reference [9], a backstepping control system with specified tracking performance using tracking error constraints and recursive fuzzy neural network (RFNN) is proposed for strict feedback nonlinear dynamic systems. Through the control of a nonlinear system and a manipulator, the effectiveness of the control method is verified. However, the real-time output of the DC microgrid controller is usually unstable, so a recursive fuzzy neural algorithm can be used to optimize the output of the DC microgrid controller to maintain the amplitude limitation and convergence of controller output.

In view of the above problems, a distributed coordinated control method of DC microgrid based on power flow calculation is designed in this article. Based on the analysis of the working mode of the DC microgrid, the droop control coefficient of the DC microgrid is calculated through power flow calculation, and then, combined with the hierarchical control strategy, a three-layer control mode is designed to enhance the feedback connection of the control process. Among them, the first layer is equipment-level control, and the second and third layers are system-level control to realize the distributed coordinated control of the DC microgrid. In the third layer control of system level, a recursive fuzzy neural network algorithm is introduced to optimize the output of the hierarchical controller, so as to maintain the amplitude limitation and convergence of output and improve dynamic response ability of the controller.

2. Analysis of Working Mode of DC Microgrid

The topology of the DC microgrid is one of the research hot spots at home and abroad. Many scholars have proposed different types of DC microgrid topologies. For example, the Royal Swedish Institute of Technology proposed a mesh structure interconnected by multiple converters; the Swedish CIGRE Institute proposed a ring network structure similar to multiterminal DC transmission. The layered structure of the DC microgrid is proposed by Aachen University of Technology according to different voltage levels. At present, common topologies mainly include parallel dendrite topology and ring network topology, as shown in Figure 1.

In Figure 1, the solid line represents the positive electrode, and the dotted line represents the negative electrode. The DC microgrid structure in this article adopts a ring network topology. In this article, the working modes of DC microgrid are summarized into five situations, the specific contents of which are as follows:

Mode (1): grid-connected operation. The power generation system runs in MPPT (Maximum Power Point Tracking) mode, the battery converter and two-way AC/DC adopt voltage sag control, and the battery works in charging or standby state according to the charge.

Mode (2): grid-connected operation. The power generation system operates in MPPT mode with a heavy load. The bidirectional AC/DC works in the current-limiting state of full power and needs to be discharged by the battery to maintain the load terminal voltage stability.

Mode (3): off-grid operation. The power generation system operates in MPPT mode, and the load terminal voltage is kept stable by the battery.

Mode (4): off-grid operation under light load (load power is less than the output power of PV MPPT mode control). The battery is full (SOC > 90%), and the power generation system operates in constant voltage mode to keep the load terminal voltage constant.

Mode (5): off-grid operation. Under heavy load (load is greater than the output power of PV MPPT control), the battery has reached the maximum discharge current or the discharge is too low (SOC < 40%), the power generation system operates in MPPT mode, and part of the load needs to be removed to keep the voltage at the load end constant, so as to ensure the power supply of important loads.

In modes (1) and (2) in the parallel operation mode and mode (3) which is the off-grid run time, the battery converter and bidirectional AC/DC converter use droop control, load voltage fluctuates with the load, and some is more sensitive to voltage change of load to maintain a constant voltage, so it needs to compensate the voltage of the load [10, 11]. In modes (4) and (5), the load terminal voltage is

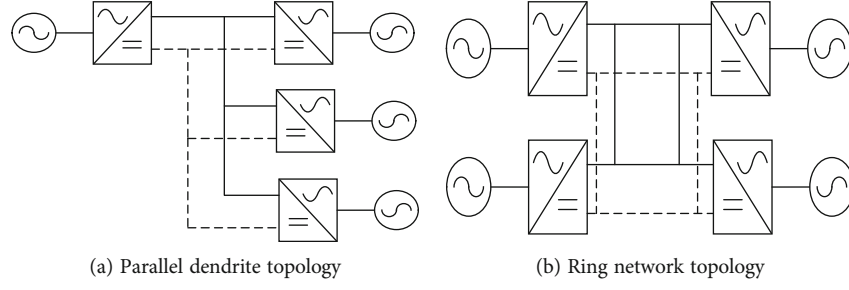(a) Parallel dendrite topology   (b) Ring network topology

FIGURE 1: Common topology of DC microgrid.

accomplished by the photovoltaic DC/DC converter. Therefore, the load terminal voltage control error needs to be transmitted to these three converters [12].

3. Power Flow Calculation

Based on the consideration of droop control, this article realizes the inwards calculation. The DC microgrid structure studied in this paper is shown in Figure 2.

In Figure 2, DC bus voltage stability is mainly achieved by the AC power source and battery. The AC power source is connected to the DC microgrid through a two-way AC/DC rectifier. The battery is connected to the DC microgrid through a DC/DC converter. The photovoltaic source is connected to the DC microgrid through a DC-DC converter and mainly operates in the MPPT mode. The load connected to the DC microgrid is set as a constant power load.

In the DC microgrid power flow, nodes can be divided into two types [13]. In this study, they are defined as W nodes and Q nodes, where the node power equation of Q node is

$$Q_{dci} = U_{dci} \sum_{j \in i} Y_{ij} U_{dcj}, \qquad (1)$$

where $j \in i$ means that node j after $\sum Y_{ij}$ must be directly connected to node i. Therefore, the nonlinear equations of the voltage of each node can be written according to the power column of each node. According to the power control of DC microgrid photovoltaic grid inverter and wind power, constant power load equipment can see as Q node, but the energy storage device (such as battery and supercapacitor) converter and two-way parallel converter can neither as Q node nor as W here to define it as node WD, and the need to meet

$$\begin{cases} Q_{dci} = U_{dci} \sum_j Y_{ij} U_{dcj}, \\ U_{dci} = U_{0i}^{\mathrm{ref}} - k_{di} I_{dci}, \\ I_{dci} = \dfrac{Q_{dci}}{U_{dci}}. \end{cases} \qquad (2)$$

After sorting out formula (2), we can get

$$U_{0i}^{\mathrm{ref}} = U_{dci} + k_{di} \sum_j Y_{ij} U_{dcj}. \qquad (3)$$

When the bidirectional converter and battery grid-connected converter is controlled by drooping and the PV is controlled by MPPT, the power flow calculation formula is as follows when the load is constant power load:

$$
\begin{aligned}
U_{\mathrm{dc\_s}}^{\mathrm{ref}} &= k_s \left[\left(\frac{1}{r_{12}} + \frac{1}{r_{13}} \right) U_{\mathrm{dc\_s}} - \frac{U_{\mathrm{dc\_b}}}{r_{12}} - \frac{U_{\mathrm{dc\_l}}}{r_{13}} \right] + U_{\mathrm{dc\_s}}, \\
U_{\mathrm{dc\_b}}^{\mathrm{ref}} &= k_b \left[\left(\frac{1}{r_{12}} + \frac{1}{r_{24}} \right) U_{\mathrm{dc\_b}} - \frac{U_{\mathrm{dc\_s}}}{R_{12}} - \frac{U_{\mathrm{dc\_p}}}{r_{24}} \right] + U_{\mathrm{dc\_b}}, \\
Q_l &= U_{\mathrm{dc\_l}} \left[\left(\frac{1}{r_{13}} + \frac{1}{r_{34}} \right) U_{\mathrm{dc\_l}} - \frac{U_{\mathrm{dc\_s}}}{r_{13}} - \frac{U_{\mathrm{dc\_p}}}{r_{34}} \right], \\
Q_{\mathrm{pv}} &= U_{\mathrm{dc\_p}} \left[\left(\frac{1}{r_{24}} + \frac{1}{r_{34}} \right) U_{\mathrm{dc\_p}} - \frac{U_{\mathrm{dc\_b}}}{r_{24}} - \frac{U_{\mathrm{dc\_l}}}{r_{34}} \right].
\end{aligned}
$$
$$(4)$$

Given the node power of Q node and the reference voltage value and sag coefficient at WD node, the voltage of each node can be obtained by solving equation (4), and then, the power flow of each branch can be obtained [14]. According to formula (4), the influence of reference voltage, droop coefficient, and line impedance must be considered in the coordinated control. For example, suppose the PV adopts the MPPT mode to output power of 5 kW, and the power of constant power load is 10 kW. If the output of the AC/DC converter and battery converter is expected to be equal, the sagging control parameters of the two converters can be set to be the same; that is, when $U_{\mathrm{dc\_s}}^{\mathrm{ref}} = U_{\mathrm{dc\_b}}^{\mathrm{ref}} = 520\,\mathrm{V}$, $k_s = k_b = 0.5$, and $r_{12} = r_{13} = r_{24} = r_{34} = 2\,\Omega$, the voltage and injected power of each node are shown in Table 1.

Obviously, bidirectional converter and battery converter controlled by voltage sag use the same reference voltage value and sag coefficient, their output is not the same, which is related to the network topology and line resistance, and the output of each converter can be changed by changing the reference voltage value and sag coefficient [15]. For example, the reference voltage of the power battery increases as $U_{\mathrm{dc\_b}}^{\mathrm{ref}} = 525\,\mathrm{V}$, other parameters are constant, the AC/DC converter and battery converter output, respectively, 2.2 kW and 3.2 kW, and output of the storage battery is the
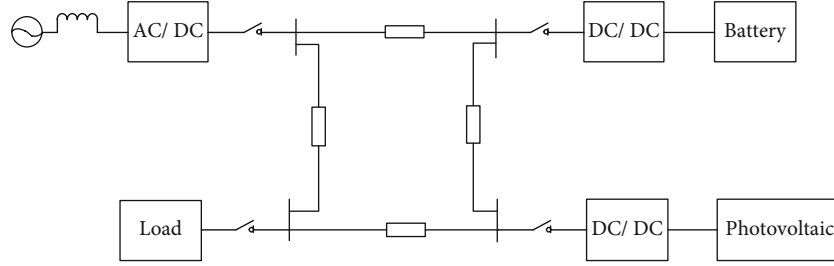
FIGURE 2: DC microgrid structure drawing.

TABLE 1: Voltage and power injection at each node.

Node	Voltage (V)	Power (kW)
AC/DC converter	515	5
Accumulator converter	518	2
Constant power load	496	10
Photovoltaic converter	517	5

proportion of increase; reducing the reference voltage of the power battery, the battery output will decrease, even by the discharge mode into charging mode. Similarly, changing the droop coefficient can also change the output of the converter.

To sum up, in the coordinated control of a DC microgrid, power flow calculation must be carried out first to verify whether the setting of the voltage reference value and sag coefficient matches the expected value of output power of each converter [16].

4. Hierarchical Coordinated Control of DC Microgrid

On the basis of the power flow calculation of the DC microgrid above, the droop control coefficient is calculated. Then, the structure and algorithm operation of the recursive fuzzy neural network are analyzed. The recursive fuzzy neural network algorithm is used to enhance the feedback connection of the control process, and a three-layer control strategy is designed.

The three-layer control strategy can be divided into device-level control and system-level control. Device-level control is based on local information to accomplish some basic control objectives similar to load distribution; system-level control is used to manage and optimize the whole system. The control objectives include the secondary regulation of DC bus voltage and the improvement of system operation efficiency, so as to achieve optimal operation. In this study, layer 1 is device-level control and layer 2 and layer 3 are system-level control.

4.1. Recursive Fuzzy Neural Network Analysis. The DC microgrid controller is a complex dynamic system with nonlinear and large time-varying characteristics. Its mechanism model is difficult to establish by conventional methods, and the stability of complex system control is particularly important in operation. Therefore, we limit and modify the output

of the DC microgrid controller through a recursive fuzzy neural network to improve its convergence and dynamic performance. The control structure diagram based on the recursive fuzzy neural network algorithm in this paper is shown in Figure 3.

4.1.1. Structure Design of RFNN Identifier. The recursive fuzzy neural network is a kind of optimal recursive neural network, which uses the recursive network to realize fuzzy inference of the output results of the neural network. It has the advantages of both recursive neural network and fuzzy logic, which not only can reflect the dynamic mapping relationship between the output results of the neural network but also has the ability of qualitative knowledge expression, which is easy to determine the structure of the network and the parameters of neurons.

The recurrent fuzzy neural network model can be stored in the form of feedback connection inside information, making the network output not only affected by the current of input data but also influenced by historical input and output data, thus forming a global or local recursive network structure, which more effectively deals with the DC microgrid nonlinear mapping problem. The network structure of the recursive fuzzy neural network (RFNN) algorithm is shown in Figure 4.

In Figure 4, the recursive fuzzy neural network is divided into six levels, namely, the input layer, the membership layer, the rule layer, the recurrent layer, the TSK fuzzy layer, and the output layer.

Layer 1 is the input layer. Each node of this layer is directly connected with the input vector, and the input value can be transmitted to the next layer. The input-output relationship of the network is

$$o_i^{(1)} = x_i. \tag{5}$$

Layer 2 is the membership layer. Usually, the membership function is a Gaussian function, and each node in this layer represents a membership function:

$$o_{ij}^{(2)} = \exp\left[-\frac{1}{2}\left(\frac{u_j^{(2)} - \mu_{ij}^p}{\sigma_{ij}^p}\right)^2\right], \quad j = 1, 2, \cdots, m, \tag{6}$$

where $\mu_{ij}^{(2)}$ represents the mean of the jth membership function of the ith input variable of the pth output mapping
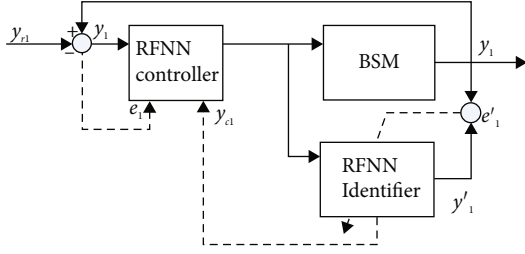
Figure 3: The control structure diagram based on recursive fuzzy neural network.
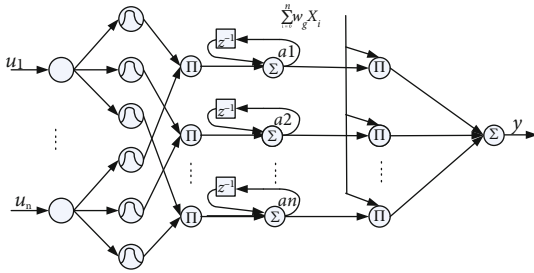

Figure 4: The network structure of RFNN.

relationship, $\sigma_{ij}^{(2)}$ represents the variance of the jth membership function of the jth input variable of the pth output mapping relationship, m is the number of membership functions of each input variable, and $o_{ij}^{(2)}$ is the ith output value.

Layer 3 is the rule layer. The activation function is the product function adopted by this layer, and a fuzzy logic rule is a node:

$$o_{pj}^{(3)} = \prod_{j=1}^{n} u_{pj}^{(3)}, \tag{7}$$

where the degree to which the input data conforms to the rule is expressed by the output strength of the jth rule node, which is $o_j^{(3)}$:

$$J_{\text{sum}} = \sum_{j=1}^{m} o_j^{(3)}, \tag{8}$$

$$J_{\text{max}} = \arg \max_{1 \leq j \leq m} \left(o_j^{(3)} \right), \tag{9}$$

$$J_{\text{min}} = \arg \min_{1 \leq j \leq m} \left(o_j^{(3)} \right), \tag{10}$$

where the minimal activated degree of the rules is J_{min} and the maximal activated degree is J_{max}, respectively.

Layer 4 is the recurrent layer. In the recursive layer, the internal variable q_j is introduced into the feedback link. The activation function of the feedback link is a linear summation function, and this link is dynamic feedback:

$$o_j^{(4)} = u_j^{(4)}(k) + p_j(k), \tag{11}$$

$$p_j(k+1) = a_j o_j^{(4)}(k), \tag{12}$$

where $a_j \in (0, 1)$ is a constant value and the output of the jth internal feedback variables is represented as $p_j(k)$ and $a_j \in (0, 1)$.

Layer 5 is the T_S fuzzy layer. Use T_S type fuzzy rules sum of each node. The operation is

$$o_j^{(5)} = o_j^{(4)} \sum_{i=0}^{n} w_{ij} x_i, \tag{13}$$

where the ith input variable is x_i and the jth consequent weight of the ith input variable is w_{ij}.

Layer 6 is the output layer. The calculation equation of nodes is

$$o = \frac{\sum_{j=1}^{m} o_j^{(5)}}{\sum_{j=1}^{m} o_j^{(4)}}, \tag{14}$$

where $i \in 1, 2, \cdots, n$; $j \in 1, 2, \cdots, m$.

4.1.2. Structure Design of RFNN Controller. The structure of the RFNN controller is the same as that of the RFNN identifier, as shown in Figure 4, and its input-output relationship expression is

$$\mathbf{Y}^{\mathbf{C}}(k) = G^C\left(X_1^C(k), X_2^C(k), u^C(k)\right), \tag{15}$$

where $u^c(k)$ is the error e between the set value of the controller output and the actual output value, $x_1^c(k)$ represent the nonlinear mapping relationship of e in the rule layer, and $x_2^c(k)$ represent the nonlinear mapping relationship of e in the T_S fuzzy layer.

4.1.3. Parameter Learning. The gradient descent method is set as the parameter learning algorithm of the RFNN controller and RFNN identifier, and their forward parameters and consequent parameters are both online learning parameters. The online learning performance index is set to

$$J = \frac{1}{2} \sum_{p=1}^{N_0} \left(y_p - y_p' \right)^2. \tag{16}$$

According to the structural design of the RFNN identifier in the previous section, as shown in Figure 4, the approximation of y_1' to y_1 is recursive convergence during parameter learning. Therefore, the analysis shows that the parameter update formula of the identifier network is

$$w_{ij}^p(k+1) = w_{ij}^p(k) - \eta_{ij}^w \frac{\partial J(k)}{\partial w_{ij}^p}, \tag{17}$$

$$\sigma_{ij}^p(k+1) = \sigma_{ij}^p(k) - \eta_{ij}^\sigma \frac{\partial J(k)}{\partial \sigma_{ij}^p}. \tag{18}$$

At time k, the gradient value of each parameter of the RFNN controller can be calculated by the gradient algorithm, and the specific calculation equation is shown in formulas (19) and (20). Since the RFNN controller adopts the same design structure as the RFNN identifier, the parameter learning of the RFNN controller also adopts the gradient descent method. The model information provided by the identifier for the output of the DC microgrid controller is shown in formula (21). Based on the model information of formula (21), formulas (17)(−)(20) are consistent with the parameter update process of the RFNN controller and will not be described in detail:

$$\frac{\partial J}{\partial w_{ij}^p} = \frac{\partial J}{\partial y_p} \frac{\partial y_p}{\partial w_{ij}^p} = \frac{1}{2} \frac{\partial \sum_{p=1}^{N_0} \left(y_p - \dot{y}_p\right)^2}{\partial y_p} \frac{\partial y_p}{\partial w_{ij}^p}$$

$$= e_p \frac{\partial \left(y_p - \dot{y}_p\right)}{\partial y_p} \frac{\partial y_p}{\partial w_{ij}^p} = -e_p \frac{o_{pj}^{(4)}}{\sum_{j=1}^{M} o_{pj}^{(4)}},$$

(19)

$$\frac{\partial J}{\partial \sigma_{ij}^p} = -e_p \frac{\partial y_p}{\partial \sigma_{ij}^p} = \frac{-2 \times e_p \left(W_{ij}^p x_i o_{pj}^{(4)} - o_{pj}^{(5)}\right) \times \left(u_j^{(2)} - \mu_{ij}^p\right)^2 \times o_{pj}^{(3)}}{\left(\sum_{j=1}^{M} o_{pj}^{(4)}\right)^2 \times \sigma_{ij}^{p\,3}},$$

(20)

$$\tilde{y}_p = \frac{-2 \times e_p \left(W_{ij}^p x_i o_{pj}^{(4)} - o_{pj}^{(5)}\right) \times \left(u_j^{(2)} - \mu_{ij}^p\right) \times o_{pj}^{(3)}}{\left(\sum_{j=1}^{M} o_{pj}^{(4)}\right)^2 \times \sigma_{ij}^p}.$$

(21)

4.1.4. Adaptive Learning Algorithm and Its Convergence Analysis. The learning rate is the most important determinant of the neural network algorithm in the learning process. A too high learning rate will cause the instability of the neural network algorithm and then make the whole learning process fail. A too low learning rate will lead to the whole learning process being too slow. To solve this problem, the adaptive change method based on the Lyapunov framework is adopted as the learning algorithm in this paper. The formula is as follows:

$$\eta^w(t) = \frac{1}{\max_k \left(\partial y_p(t)/\partial w_{ij}^p\right)^2},$$

(22)

$$\eta^\sigma(t) = \frac{1}{\max_k \left(\partial y_p(t)/\partial \sigma_{ij}^p\right)^2}.$$

(23)

On the premise of ensuring the convergence of neural networks, in order to speed up the convergence process of the neural network, this paper adopts the adaptive variable learning rate. The convergence proof of adaptive learning rate can be obtained by constructing the Lyapunov function. Firstly, the Lyapunov function is constructed, as shown in the following formula:

$$V(t) = J(t) = \frac{1}{2} \sum_{p=1}^{N_0} e_p^2.$$

(24)

It can be obtained from formula (24):

$$\Delta V(t) = V(t+1) - V(t) = \frac{1}{2} \sum_{p=1}^{N_0} \left(e_p^2(t+1) - e_p^2(t)\right).$$

(25)

When $\Delta V \le 0$, the neural network algorithm is convergent and stable, which is determined by the Lyapunov stability principle. According to the model structure of the recursive fuzzy neural network algorithm, the following equation can be obtained:

$$\Delta V(t) = \Delta V_1(t) + \Delta V_2(t) + \cdots + \Delta V_{N_0}(t),$$

(26)

$$\Delta V_p(t) = V_p(t+1) - V_p(t) = \frac{1}{2} \left(e_p^2(t+1) - e_p^2(t)\right).$$

(27)

According to Reference [9], formula (28) can be obtained:

$$\Delta e(t) = e(t+1) - e(t) \cong \left[\frac{\partial e(t)}{\partial X}\right]^T \Delta X,$$

(28)

where

$$\left[\frac{\partial e(t)}{\partial X}\right] = \left[\frac{\partial e(t)}{\partial w} \frac{\partial e(t)}{\partial \sigma}\right],$$

(29)

$$\Delta X = \left[\Delta w \, \Delta \sigma\right]^T.$$

(30)

Theorem 1. *When it is satisfied,*

$$\eta^w(t) = \frac{2}{\max_k \left(\partial y_p(t)/\partial w_{ij}^p\right)^2},$$

(31)

$$\eta^\sigma(t) = \frac{2}{\max_k \left(\partial y_p(t)/\partial \sigma_{ij}^p\right)^2}.$$

(32)

This neural network learning algorithm is convergent and stable.

Proof of Theorem 1. Formulas (33) and (34) can be obtained from formulas (17), (20), (26), and (28):

$$\Delta e_p(t) = -e_p(t) \left[\sum_{j=1}^{N_p} \sum_{i=0}^{n} \eta_{ij}^w \left(\frac{\partial y_p(t)}{\partial w_{ij}^p}\right)^2 + \sum_{j=1}^{N_p} \sum_{i=0}^{n} \eta_{ij}^\mu \left(\frac{\partial y_p(t)}{\partial \mu_{ij}^p}\right)^2 + \sum_{j=1}^{N_p} \sum_{i=0}^{n} \eta_{ij}^\sigma \left(\frac{\partial y_p(t)}{\partial \sigma_{ij}^p}\right)^2\right],$$

(33)

$$\Delta V_p(t) = -\frac{1}{2} e_p^2(t) \left\{ \sum_{j=1}^{N_p} \sum_{i=0}^{n} \eta_{ij}^w \left(\frac{\partial y_p(t)}{\partial w_{ij}^p} \right)^2 \left[2 - \eta_{ij}^w \left(\frac{\partial y_p(t)}{\partial w_{ij}^p} \right)^2 \right] \right.$$
$$+ \sum_{j=1}^{N_p} \sum_{i=1}^{n} \eta_{ij}^\mu \left(\frac{\partial y_p(t)}{\partial \mu_{ij}^p} \right)^2 \left[2 - \eta_{ij}^\mu \left(\frac{\partial y_p(t)}{\partial \mu_{ij}^p} \right)^2 \right]$$
$$\left. + \sum_{j=1}^{N_p} \sum_{i=1}^{n} \eta_{ij}^\sigma \left(\frac{\partial y_p(t)}{\partial \sigma_{ij}^p} \right)^2 \left[2 - \eta_{ij}^\sigma \left(\frac{\partial y_p(t)}{\partial \sigma_{ij}^p} \right)^2 \right] \right\}. \tag{34}$$

$e_p^2 \geq 0$ can be obtained according to equation (34). For $\Delta V \leq 0$, formula (34) in braces is not less than zero. It is obtained:

$$\eta_{ij}^w(t) < \frac{2}{\left(\partial y_p(t) / \partial w_{ij}^p \right)^2}, \tag{35}$$

$$\eta_{ij}^\sigma(t) < \frac{2}{\left(\partial y_p(t) / \partial \sigma_{ij}^p \right)^2}. \tag{36}$$

For each type of parameter, in order to unify the learning rate standard, the unified standard of the learning rate of each type of parameter can be formulated by

$$\eta^w(t) < \frac{2}{\max_k \left(\partial y_p(t) / \partial w_{ij}^p \right)^2}, \tag{37}$$

$$\eta^\sigma(t) < \frac{2}{\max_k \left(\partial y_p(t) / \partial \sigma_{ij}^p \right)^2}. \tag{38}$$

Therefore, when the change of learning rate satisfies formulas (37) and (38), the algorithm is convergent and stable, and Theorem 1 is correct. □

4.2. Layered Coordinated Control Process Design. On the basis of the above analysis of the recursive fuzzy neural network, the recursive fuzzy neural network algorithm is used to enhance the feedback connection of the control process, so as to form a three-layer coordinated control strategy.

4.2.1. Layer 1 Control. In the first layer control, each unit only depends on its own injected power and port voltage and other internal information, according to their own droop characteristics to carry out load distribution, so as to achieve supply and demand power balance [17, 18]. As for the uncontrollable clean energy, such as photovoltaic power supply, which generally generates electricity according to the maximum power, it can be considered as a whole with energy storage as controllable clean energy. In this case, the droop method can be applied for control.

The droop control can be expressed as a linear function of voltage and power. Therefore, the governing equation of the first-layer control is set as follows:

$$\begin{cases} v_0 = V_{\text{ref}} - d_i P_i + \Delta v, \\ d_i = d_{i0} - \Delta d. \end{cases} \tag{39}$$

In the formula, v_0 represents the voltage value of the current operating point; V_{ref} represents the reference voltage of sag control; d_i represents the improved sag coefficient; d_{i0} represents the original reference value of sag coefficient, which is proportional to their respective capacities; and Δv and Δd represent the changes in output voltage and sag coefficient, respectively, which are determined by the control results of the second and third layers, respectively.

4.2.2. Layer 2 Control. In the second layer, each control unit calculates the average voltage value of the system through the finite time consistency algorithm based on the voltage information of itself and its connected communication units.

The voltage iteration formula of control unit i is

$$v_i(m + 1) = w_{ii}(m)v_i(m) + \sum_{j \in i} w_{ij}(m)v_j(m), \tag{40}$$

where $v_i(m)$ represents the output voltage value calculated by element i after the mth iteration and $w_{ii}(m)$ and $w_{ij}(m)$ represent weights, which can adapt to the changes of system communication topology and meet the requirements of "plug and play" of distributed power supply. The average uniform voltage of each unit is obtained after g iterations, and its value is shown in

$$\bar{v} = v_1^g = v_2^g = \cdots = v_i^g = \frac{1}{n} \sum_{i=0}^{n} v_{i0}, \tag{41}$$

where $\bar{v}$ represents the average voltage, v_i^g represents the voltage value calculated by element i after the gth iteration, and v_{i0} represents the initial voltage of each element. At the end of iteration, in view of the problem of voltage deviation caused by droop control, the recursive fuzzy neural network algorithm is used to fuzzy the voltage of each generation unit to realize the voltage correction and control. The voltage deviation Δv_i is obtained by comparing the average voltage with the given reference voltage. The calculation process is as follows:

$$\Delta v_i = \left(K_{pv} + \frac{K_{iv}}{s} \right)(V_{\text{ref}} - \bar{v}), \tag{42}$$

where K_{pv} and K_{iv} represent fuzziness coefficient and membership coefficient, respectively.

4.2.3. Layer 3 Control. The primary objective of layer 3 control is to minimize the cost of generating electricity. In this paper, uncontrollable clean energy, such as wind power and photovoltaic, is matched with energy storage units to change the situation that wind power and photovoltaic are unimpeachable. Therefore, the distributed power supply in the DC microgrid can be divided into internal combustion power supply and clean energy for discussion.

For the internal combustion type generation unit, the fuel cost is much larger than the converter loss, so the cost function mainly considers both the fuel cost and the maintenance cost. For the ith internal combustion type generation unit, P_{Gi} is its output power, and the cost function is shown as follows:

$$C_{GiP_{Gi}} = M_{Gi}P_{Gi} + F_{Gi}\left(\alpha_{Gi} + \beta_{Gi} + \lambda_{Gi}P_{Gi}^2\right), \qquad (43)$$

where C_{Gi} represents the cost of power generation, M_{Gi} represents the maintenance cost per unit power generation unit i of the internal combustion engine, F_{Gi} represents the cost of fuel per kilo calorie, and α_{Gi}, β_{Gi}, and λ_{Gi} represent the fuel cost coefficient of the gas turbine.

Clean energy generally outputs power through the converter; at this time, the converter loss value becomes an important factor affecting the cost of power generation. Therefore, the cost function of controllable clean energy of fuel cells includes three parts: fuel cost, maintenance cost, and converter loss. For the jth controllable clean energy generation unit, P_{Qj} is its output power, and the cost function can be expressed as

$$C_{Qj}\left(P_{Qj}\right) = \left(M_{Qj} + F_{Qj}\right)\left(a_{Qj} + b_{Qj}P_{Qj} + c_{Qj}P_{Qj}^2\right). \qquad (44)$$

In formula (44), P_{Qj} represents the output power unit of the converter, M_{Qj} represents the maintenance cost per unit power of the clean energy generation unit j, F_{Qj} represents the cost per unit power of the fuel cell, and a_{Qj}, b_{Qj}, and c_{Qj} represent the loss coefficient of the converter, corresponding to the no-load loss, resistance loss, and power device loss of the converter, respectively.

In the cost of wind power and photovoltaic power generation, fuel costs are not taken into account, and the cost of energy storage is mainly taken into account in terms of maintenance costs. Therefore, the cost functions of both can be expressed in formula (44), except that the value of PQ_j is 0 at this time. Since the whole composition of scenery and energy storage is taken into account in this paper, the overall cost function is finally expressed in the form of formula (44).

In the process of stable operation, each generation unit should also meet a series of constraints, including supply and demand power balance constraints and maximum and minimum power constraints. Formula (45) is the constraint function:

$$\begin{cases} \sum_{i=1}^{m} P_{Gi} + \sum_{j=1}^{n} P_{Qj} - \sum_{k=1}^{l} P_{Lk} = 0, \\ P_{Gi,\min} \leq P_{Gi} \leq P_{Gi,\max}, \\ P_{Qj,\min} \leq P_{Qj} \leq P_{Qj,\max}, \end{cases} \qquad (45)$$

where P_{Lk} represents the power consumed by the load.

When all generating units and loads meet the inequality constraint conditions, the fuzzy correction value of the
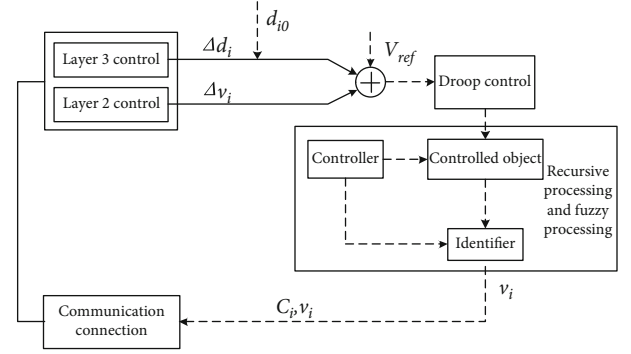

FIGURE 5: Block diagram of distributed coordinated control of DC microgrid.

droop coefficient can be obtained after processing by the recursive fuzzy neural network algorithm. The calculation process is as follows:

$$\Delta d_i = \left(K_{pc} + \frac{K_{ic}}{s}\right) \times C. \qquad (46)$$

In the formula, K_{pc} and K_{ic} represent the correction coefficients of the recursive layer and the fuzzy layer, respectively, and C represents the average cost, that is, the cost of each generation unit after iterative convergence.

This enables layer 3 control. It can be seen that the units with high generation costs bear less output power, so as to realize the economic operation of the system while satisfying the proportional distribution of load.

To sum up, this study carried out distributed and coordinated control for the DC microgrid based on the above working mode analysis and power flow calculation results. The recursive fuzzy neural network algorithm is used to enhance the feedback connection of the control process, and the three-layer coordinated control can be formed [19].

In the recursive fuzzy neural network, an identifier and a controller are set. Among them, the controller can output the control signal according to the system error, combined with the adaptive control law, and is used for the controlled object, making the output result of the object load the expected value range. The identifiers can identify the controlled objects and provide object information for the adaptive adjustment of the controller.

Because processing layer 3 of the recursive fuzzy neural network contains the dynamic feedback connection link, when using the discriminator to identify the controlled object, only the output value of the controlled object at the previous time and the control signal value at the current time are used as the input of the network, which can greatly control the process.

Thus, the specific idea of the layered coordinated control method for DC microgrid based on the recursive fuzzy neural network algorithm is shown in Figure 5.

Before the method is started, each unit is controlled by the traditional droop control method. With this method enabled, each cell relies on its local controller to exchange information with its neighboring cells, including its own
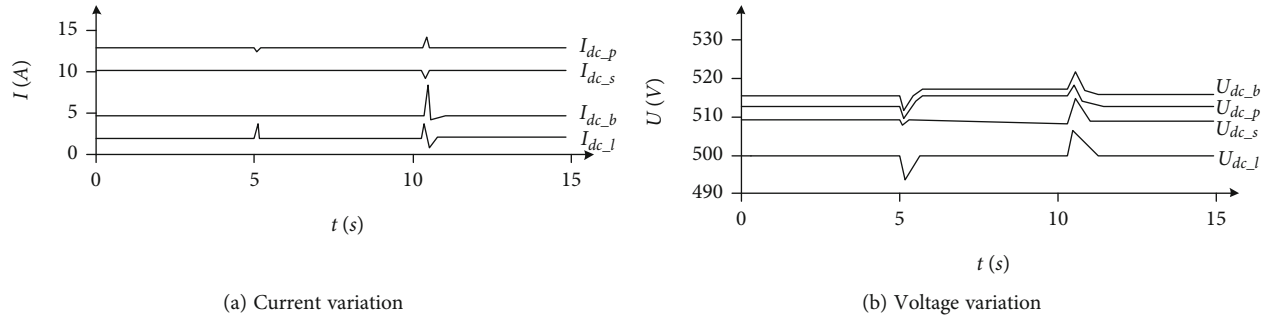
(a) Current variation

(b) Voltage variation

FIGURE 6: Changes in the current and voltage of each port during grid-connected–off-grid–grid-connected switching.

operating voltage and cost. After the initial cost is iteratively averaged in the third layer of control, Δd_i is used to modify the sag coefficient to obtain d_i, and the new operating point voltage is obtained. The voltage was substituted into control layer 2 to calculate the average voltage, then compared with V_{ref} to get the voltage deviation Δv_i, and then substituted Δv_i into formula (39) to get the final control equation. Through the final control equation, each control unit can realize the load distribution based on the minimum generation cost and finally effectively maintain the bus voltage stability.

5. Experiment and Analysis

In order to verify the feasibility of the hierarchical coordinated control method of DC microgrid based on the recursive fuzzy neural network algorithm designed above, the following experiments were designed in the MATLAB platform to verify.

The experiment takes a DC microgrid as the object, and its operation is as follows: the DC bus voltage of the DC microgrid is 500 V; the two-way AC/DC converter is connected to the 220 V AC grid through a 2 : 1 transformer, with a capacity of 5 kW, a reference voltage of 515 V, and a sag coefficient of 0.5. Of photovoltaic power generation unit capacity of 5 kW, the energy storage unit adopts the rated power of 3 kW battery, its capacity is 220 V/50 Ah, the rated discharge current is 10 A, battery SOC upper and lower are 90% and 40%, respectively, the battery converter of three reference voltage values is 515 V, 512.55 V, and 510 V, corresponding to the discharging and charging, automatic mode, and droop coefficient of 0.25, and dead zone limit is +/-2.5 V, allowing the load side of plus or minus 10 V DC bus voltage variation.

5.1. Check the Effect of Seamless Switch Control of Grid-Connected–Off-Grid–Grid-Connected. Firstly, the method in this paper is used to carry out grid-off grid-connected seamless switching control for DC microgrid, and its control effect is tested. When the load resistance is 40 Ω (12.5 A), the photovoltaic converter has been working in MPPT mode; the port, the change of the voltage, and current are shown in Figure 6.

As can be seen from Figure 6, the AC/DC bidirectional converter operates in the voltage sag control mode during
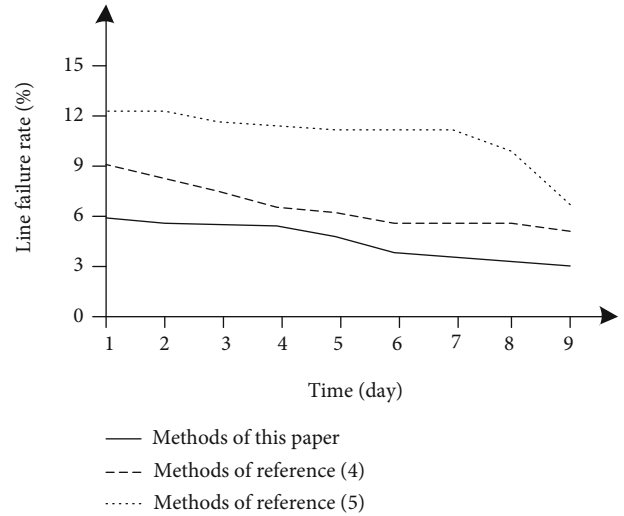

FIGURE 7: The line failure rate is compared under different control methods.

0-5 s, and the battery converter reference voltage is 514 V and is in the automatic switching mode. At this point, due to the relatively light load, the battery is in standby mode. After 5 s, disconnect the AC/DC bidirectional converter, the DC microgrid changes from grid-connected operation to off-grid operation, the battery automatically switches to discharge mode, and the load terminal voltage is maintained at 500 V. At 10.5 s, the grid connection is restored, and the AC/DC bidirectional converter operates in voltage sag mode. The voltage at the negative end is maintained at 500 V. After a short transient process, the battery converter returns to a standby state. In the grid–off-grid switching, the operating mode of each converter is automatically switched. During the switching process, the voltage of each port will fluctuate. Under the steady-state condition that the voltage fluctuation of the load terminal is less than 10 V, both the grid-connected and off-grid terminals will remain at 500 V. Thus, it can be shown that this paper has achieved a better control effect. It can be seen from the figure that after the step of voltage and current, they both can quickly return to a stable state. It shows that after the improvement of the recursive fuzzy neural network algorithm, the DC microgrid control system has good robustness, stability, and fast convergence speed.

5.2. Check the Failure Rate of DC Microgrid Line. On this basis, in order to further highlight the effectiveness of the proposed method, the application performance of the proposed method, the Reference [6] method, and the Reference [7] method is verified by taking the failure rate of the DC microgrid line as the index. The line failure rate can reflect the operation safety of the DC microgrid, and it is a key index to evaluate the control effect and reflect the effectiveness of the control method.

A line in the experimental area was randomly selected as the experimental object to verify the failure rate of DC microgrid lines under the control of different methods. The results are shown in Figure 7.

According to the results shown in Figure 7, under the control of different methods, the failure rate of the circuit decreases over time. Under the control of methods of Reference [6], the fault rate of the circuit is slightly higher than that of the methods of this paper. Under the control of methods of Reference [7], the line failure rate is obviously higher. Under the control of methods of this paper, the line failure rate decreases from 6% to 3%. The above results fully demonstrate that the methods of this paper can realize effective coordinated control of fault frequency of DC microgrid lines, so as to ensure the operation safety of the DC microgrid.

6. Conclusion

In this article, a hierarchical coordinated control method of DC microgrid based on the recursive fuzzy neural network algorithm is designed. On the basis of droop control, the coordinated and optimal control of the DC microgrid is realized through a three-layer hierarchical control structure, so as to achieve the purpose of stable operation of the DC microgrid. At the same time, the recursive fuzzy neural network algorithm is used to optimize the system-level control of the third layer in the hierarchical control structure, so as to ensure the real-time amplitude limiting, convergence, and stability of the DC microgrid controller. The experimental results show that under the control of the intelligent control algorithm in this paper, the current and voltage changes of each port of the DC microgrid are relatively stable in the process of off-grid switching, and the power grid line fault rate is low, which fully proves the effectiveness of this method. In the following research, we can further optimize the method in this paper from the perspective of shortening the control reaction time, so as to comprehensively improve its application performance.

Data Availability

No data were used to support this study.

Conflicts of Interest

The authors declare that there are no conflicts of interest regarding the publication of this article.

Acknowledgments

References

[1] R. C. Zhang, D. J. Zhai, and Y. Zhang, "DC microgrid distributed coordinated control strategy including hybrid energy storage system," *Journal of Ordnance Equipment Engineering*, vol. 41, no. 4, pp. 232–236, 2020.

[2] Y. Mi, Y. W. Wu, H. P. Ji, F. Yang, and C. S. Wang, "Coordinative control based on dynamic load allocation among multiple energy storages for is landed DC microgrid," *Electric Power Automation Equipment*, vol. 37, no. 5, pp. 170–176, 2017.

[3] J. D. Wu, K. Y. Wang, X. Huang, C. Qi, G. J. Li, and Y. Zhang, "Distributed coordinated control scheme of parallel DC-DC converters in isolated DC microgrids," *Power System Protection and Control*, vol. 48, no. 11, pp. 76–83, 2020.

[4] B. Liu, "Logistics distribution route optimization model based on recursive fuzzy neural network algorithm," *Computational Intelligence and Neuroscience*, vol. 2021, 10 pages, 2021.

[5] G. Tang, X. Zheng, S. Liu, Y. L. Gu, Y. Lu, and P. Qiu, "Novel DC voltage control strategy for multi terminal flexible DC transmission system," *Power system automation*, vol. 37, no. 15, pp. 125–132, 2013.

[6] Y. L. Li, P. Dong, M. B. Liu, and Y. Lin, "Distributed coordinated control of DC microgrid based on finite-time consensus algorithm," *Automation of Electric Power Systems*, vol. 42, no. 16, pp. 96–103, 2018.

[7] W. Q. Xie, M. X. Han, H. J. Wang, R. Li, and M. Wu, "Multi-source coordinated control strategy of DC micro-grid based on virtual voltage," *Proceedings of the CSEE*, vol. 38, no. 5, pp. 1408–1418, 2018.

[8] F. F. M. El-Sousy, "Adaptive hybrid control system using a recurrent RBFN-based self-evolving fuzzy-neural-network for PMSM servo drives," *Applied Soft Computing*, vol. 21, no. 8, pp. 509–532, 2014.

[9] S. I. Han and J. M. Lee, "Recurrent fuzzy neural network backstepping control for the prescribed output tracking performance of nonlinear dynamic systems," *ISA Transactions*, vol. 53, no. 1, pp. 33–43, 2014.

[10] C. Dou, Y. Dong, J. M. Guerrero, X. Xie, and S. Hu, "Multi-agent system-based distributed coordinated control for radial DC microgrid considering transmission time delays," *IEEE Transactions on Smart Grid*, vol. 8, no. 5, pp. 2370–2381, 2017.

[11] B. K. Chaitanya, A. Yadav, and M. Pazoki, "Wide area monitoring and protection of microgrid with DGs using modular artificial neural networks," *Neural Computing and Applications*, vol. 32, no. 7, pp. 2125–2139, 2020.

[12] H. M. Peng, L. Chang, Y. C. Guo, S. H. Li, and H. Li, "Dynamic interval power flow calculation of microgrid under master-slave control," *Power System Technology*, vol. 42, no. 1, pp. 195–202, 2018.

[13] K. M. Bhargavi and N. S. Jayalakshmi, "Leader–follower-based distributed secondary voltage control for a stand-alone PV and wind-integrated DC microgrid system with EVs," *Journal of Control, Automation and Electrical Systems*, vol. 17, no. 3, pp. 1–14, 2020.

[14] G. Y. Lee, B. S. Ko, J. Cho, and R. Y. Kim, "A distributed control method based on a voltage sensitivity matrix in DC microgrids with low-speed communication," *IEEE Transactions on Smart Grid*, vol. 10, no. 4, pp. 3809–3817, 2019.

[15] X. Liu, Z. Xie, Q. Sun, and Z. Wang, "A novel protection scheme against fault resistance for AC microgrid," *Mathematical Problems in Engineering*, vol. 2017, Article ID 8419257, 2017.

[16] Y. Han, Y. Pu, Q. Li et al., "Coordinated power control with virtual inertia for fuel cell-based DC microgrids cluster," *International Journal of Hydrogen Energy*, vol. 44, no. 46, pp. 25207–25220, 2019.

[17] L. Gao, L. Yao, H. Ren, and J. M. Guerrero, "A DC microgrid coordinated control strategy based on integrator current-sharing," *Energies*, vol. 10, no. 8, pp. 1116–1123, 2017.

[18] G. H. Philipo, Y. A. C. Jande, and T. Kivevele, "Clustering and fuzzy logic-based demand-side management for solar microgrid operation: case study of Ngurudoto microgrid, Arusha, Tanzania," *Advances in Fuzzy Systems*, vol. 2021, Article ID 6614129, 2021.

[19] R. Atassi and K. Yang, "An integrated neutrosophic AHP and TOPSIS methods for assessment renewable energy barriers for sustainable development," *International Journal of Neutrosophic Science*, vol. 18, no. 2, pp. 157–173, 2022.